Electronic structure and optical properties of cubic $Ce_{0.5}La_{0.5}AlO_3$ under the different pressures: a DFT study

DAN LI*
Department of Optics and Electronic Information, Hubei University of Education, Wuhan, 430205 China

Using the Heyd-Scuseria-Ernzerhof screened hybrid functional, we systematically investigate the electronic structure and optical properties of cubic $Ce_{0.5}La_{0.5}AlO_3$ under varying pressure. The lattice constant decreases significantly as pressure increases. For electronic properties, the band gap exhibits a steady reduction with rising pressure. Meanwhile, the bandwidths of two higher valence bands and conduction band increase, though the lowest valence band remains unaffected. Optically, pressure enhances the strongest peak of the imaginary part of the dielectric constant, induces a slow increase in the static dielectric constant, and causes distinct blue-shift in the prominent peaks of the absorption coefficient, reflectivity, and energy-loss function.

(Received June 17, 2025; accepted February 4, 2026)

Keywords: Electronic structure, Optical properties, Pressure, Heyd-Scuseria-Ernzerhof screened hybrid functional

1. Introduction

$LaAlO_3$ is an active perovskite oxide material with extraordinary dielectric properties in experimental and theoretical studies. It is widely used in ferroelectric thin films, microwave devices, dielectric resonators, high-frequency capacitors, and high-temperature superconductor manufacturing [1–6]. Due to the high k-value, $LaAlO_3$ plays a crucial role in the production of fuel cell electrolytes, automobile catalytic converters, and field transistors [7–10].

In addition, finding new heavy ion materials suitable for use as scintillators is very important in physics and chemistry today. At present, scintillators have been applied in fields such as geological survey, environmental monitoring, oil well logging, high-energy physics, industrial flaw detection, and astronomy [11]. One of the promising scintillation materials is aluminum perovskite [12]. Currently, one of the most famous perovskite scintillators is Ce-doped $LaAlO_3$, whose growth technology [13] has been well-established due to its extensive use as a substrate for thin film epitaxial growth [3].

$LaAlO_3$ has been widely studied due to its high band-gap value [14, 15]. By doping elements such as Sr, Mg, and Ce [16, 17] into La or Al sites, band-gap tailoring plays a key role in modulating the material's physical and chemical properties. In order to explore the doping effect in $LaAlO_3$, many experimental [16–24] and theoretical [25–30] studies have been conducted to improve the electronic, structural, and optical properties of the $LaAlO_3$.

There are also many studies on the optical absorption and luminescence of Ce-doped $LaAlO_3$. X. Zeng *et al.* grew Ce-doped $LaAlO_3$ single crystals using Czochralski method and characterized them via infrared transmission spectra and ultraviolet/visible/near-IR absorption spectra [13]. J. Pejchal *et al.* used micro-pulling-down method to grow Ce-doped $LaAlO_3$ perovskite single crystals and found that their radioluminescence efficiency was very low, with the observed emission attributed to defects [31]. V. Laguta *et al.* also performed detailed investigations of Ce^{3+} EPR and NMR in the $La_{1-x}Ce_xAlO_3$ solid solutions with Ce concentrations ranging from $x = 0.001$ up to $x = 1.0$ [32].

In the situ synchrotron powder diffraction study, it was found that $Ce_{1-x}La_xAlO_3$ solid solution in the $CeAlO_3$-$LaAlO_3$ pseudo-binary system exhibited high-temperature cubic and low-temperature tetragonal modifications. When $x = 0.5$, $Ce_{1-x}La_xAlO_3$ exhibited a simple cubic perovskite structure belonging to the *Pm-3m* space group at $T = 1173$ [33] at ambient pressure. When the external pressure reached 13.2 GPa, the pressure provided sufficient driving force to overcome the energy barrier required for the structural reconstruction. The synchrotron X-ray diffraction experiments confirmed that $LaAlO_3$ transforms from the rhombohedral phase to the cubic phase at approximately 13.2 GPa [33]. $Ce_{0.5}La_{0.5}AlO_3$, as a solid solution of $LaAlO_3$ and $CeAlO_3$, reached the critical energy condition for the phase transition at this pressure. After the phase transition, the cubic structure of $Ce_{0.5}La_{0.5}AlO_3$ forms a stable ionic bond framework. The Ce^{3+}/La^{3+} ions at the A sites coordinate with the Al^{3+} ions at the B sites in a regular octahedral manner with O^{2-} ions, and the uniform distribution of atomic forces significantly reduces the lattice energy [34]. High-pressure studies have shown that the cubic phase of $LaAlO_3$ remains stable under a pressure of 63 GPa and does not undergo a secondary phase transition [33]. Moreover, $Ce_{0.5}La_{0.5}AlO_3$, which has a similar perovskite structure, also exhibits excellent long-term stability under the high pressure. In terms of mechanical stability, the elastic constants of the

cubic $Ce_{0.5}La_{0.5}AlO_3$ satisfy $C_{11} > 0$, $C_{12} > 0$, $C_{44} > 0$, and $C_{11} - C_{12} > 0$. Therefore, this material possesses the mechanical stability of a cubic crystal [35].

Since the physical properties of the material change significantly with pressure, we decided to theoretically investigate the structural and optoelectronic properties of the $Ce_{0.5}La_{0.5}AlO_3$ compound under varying pressure conditions in detail.

2. Method of calculation

According to the report by L. Vasylechkoa *et al.*, the space group of the cubic pervoskite $Ce_{0.5}La_{0.5}AlO_3$ is *Pm-3m* at around $T = 1173$ K [33] with the position of Ce/La atom being (0.25, 0.25, 0.25), the position of Al atom is (0, 0, 0), and the position of O atom being (0.5, 0, 0). In this calculation, we used a $2\times1\times1$ supercell and replaced half of the Ce atoms with La atoms.

Our calculation was based on the density functional theory (DFT) with the generalized gradient approximation (GGA) in the CASTEP codes [36, 37], which was used to solve the Kohn-Sham equation with the minimum of the function of total energy. Compared with the actual band gap, the semilocal approximation to the exchange-correlation energy leads to the smaller calculated one, so we used the hybrid density functionals including a certain amount of Hartree-Fock exchange to increase the band gap [38–43]. To investigate the variations in electronic and optical properties under different pressure conditions, the Heyd-Scuseria-Ernzerhof screened hybrid functional with norn-conserving pseudopotential was employed [44]. Here, the electronic configuration of cubic $Ce_{0.5}La_{0.5}AlO_3$ for Ce was $4f^15p^65d^16s^2$, for La was $5p^65d^16s^2$, for Al was $3s^23p^1$, and for O was $2s^22p^4$. A discrete plane-wave basis set with a cutoff energy of 300 eV was used to expand the valence wave function. For the calculations of electronic and optical properties, $9\times9\times9$ and $11\times11\times11$ K points were set by Monkhorst–Pack method for integration over Brillouin-zone (BZ). The parameters of the self-consistence energy calculations were as follows: the convergence threshold of total energy was 1×10^{-5} eV/atom, the maximum force of per atom was 0.01 eV/Å, the maximum stress was 0.02 GPa, the maximum displacement of atom was 0.0005 Å, and the tolerance was 1×10^{-6} eV/atom.

3. Results and discussions

3.1. Structural properties analyses

Structure optimization was performed prior to single-point energy calculations. The optimized lattice constant of cubic $Ce_{0.5}La_{0.5}AlO_3$ at ambient pressure is $a = 3.79796$ Å. This value is in good agreement with the result of the previous report [33]. Therefore, based on the optimized structure, the following calculations of the electronic structure and optical properties under different pressures with the same method are highly reliable. Fig. 1 shows the dependence of the lattice constant of $Ce_{0.5}La_{0.5}AlO_3$ on pressure. It can be clearly seen that the lattice constant sharply decreases, this downward trend is attributed to the fact that increased pressure enhances atomic interactions, thereby reducing the interatomic distance [45].

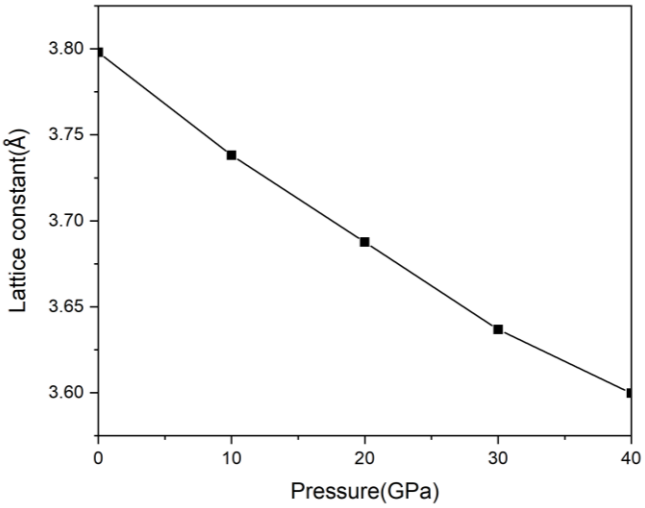

Fig. 1. Variation of lattice constant with different pressures

3.2. Electronic properties analyses

To investigate the electronic characteristics of cubic $Ce_{0.5}La_{0.5}AlO_3$ under different pressure conditions, their respective band structures are presented in Fig. 2. Analysis reveals that the valence band maximum (VBM) and conduction band minimum (CBM) of the compound coincide at the G point within the first Brillouin zone, indicating it is direct band gap material. The theoretical value of band gap of the cubic $Ce_{0.5}La_{0.5}AlO_3$ at ambient pressure is 2.55 eV. As pressure increases, the band gap deceases, as shown in Fig. 3 [45].

Figs. 4 and 5 show the total density of states (TDOS) and the corresponding partial density of states (PDOS) of cubic $Ce_{0.5}La_{0.5}AlO_3$ under different pressures, with the PDOS for Ce, La, Al and O atoms are presented in Figs. 5a-5d, respectively. The low valence band, ranging from -33.92 eV to -30.02 eV, is mainly occupied by s-states of Ce and La. Strong hybridization occurs between the middle and high valence bands. The middle valence band, spanning from -20.75 eV to -12.17 eV, mainly originates from O-s states, Al-s/p states, Ce-p and La-p states. The high valence band ranges from -9.36 eV to the Fermi energy dominated by Ce-s/p/d, La-s/p/d states, Al-s/p states, and O-p states. The conduction band is mainly come from Ce-d/f and La-d states [46]. The increase in pressure for the cubic $Ce_{0.5}La_{0.5}AlO_3$ increases the bandwidth of the middle valence band, high valence band, and conduction band.

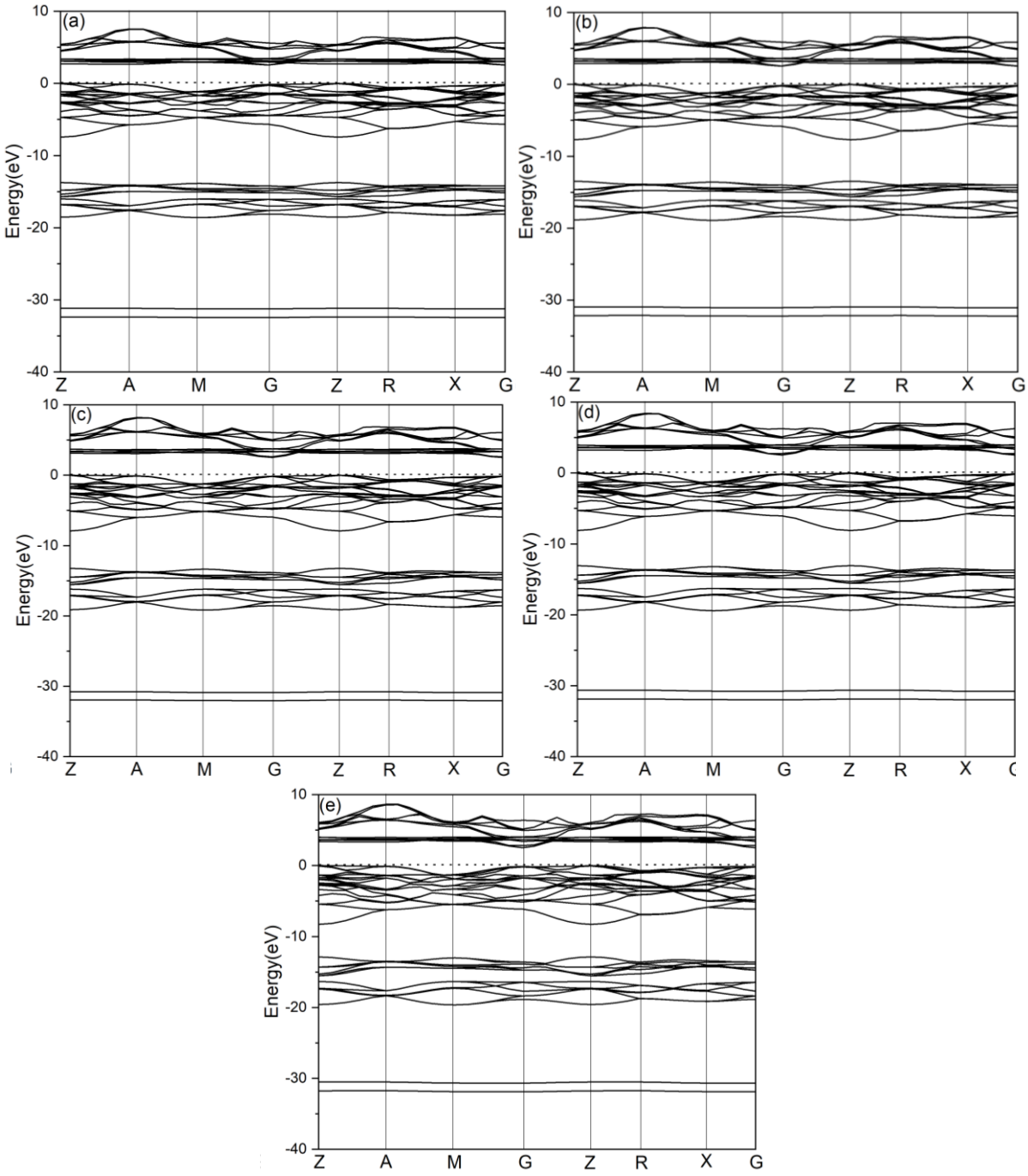

Fig. 2. Band structures of $Ce_{0.5}La_{0.5}AlO_3$ under (a) 0GPa, (b) 10GPa, (c) 20GPa, (d) 30GPa and (e) 40GPa

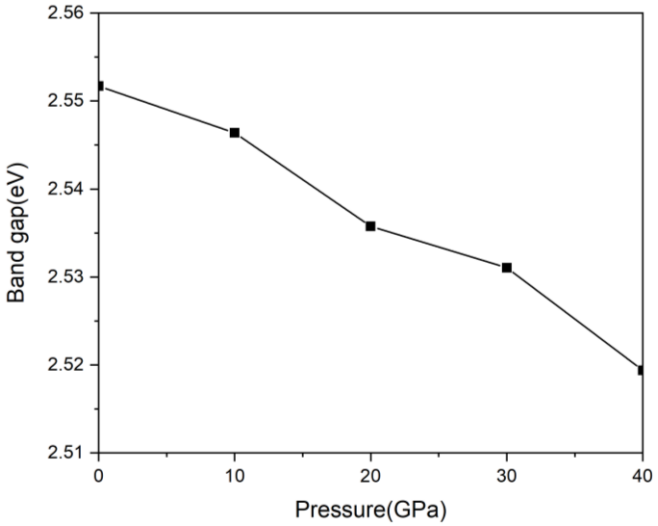

Fig. 3. Variation of band gaps with different pressures

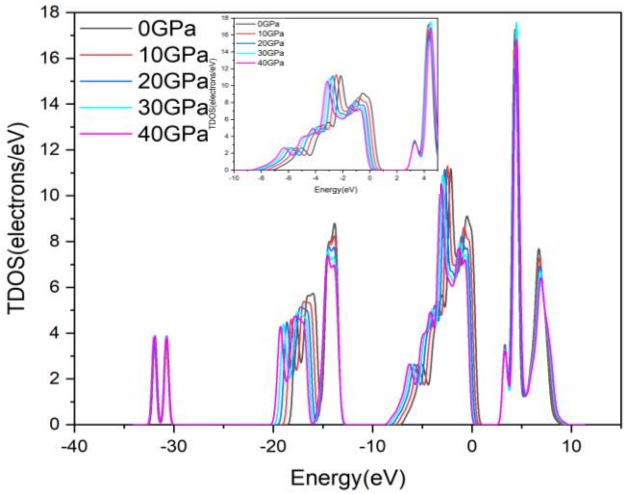

Fig. 4. Total density of states of $Ce_{0.5}La_{0.5}AlO_3$. The insert shows the close-up figure of the total density of states from -10 to 5 eV (colour online)

3.3. Optical properties analyses

The electronic and optical properties of cubic $Ce_{0.5}La_{0.5}AlO_3$ are inherently interconnected, with pressure-induced band-gap tailoring serving as the core bridge that modulates their correlation. Pressure induces a significant reduction in the lattice constant of $Ce_{0.5}La_{0.5}AlO_3$. This structural compression directly narrows the material's band-gap, and increases the widths of the middle and high valence bands as well as the conduction band, and reshapes the density of states (DOS) [33]. These electronic changes directly modulate the energy threshold, transition probability, and state energy levels of electron-photon interactions, thereby governing the intensity, spectral position, and functional behavior of optical properties. We systematically studied the dielectric function, absorption coefficient, reflectivity, and energy-loss function of cubic $Ce_{0.5}La_{0.5}AlO_3$ under different pressures.

Dielectric function $\varepsilon(\omega)$ can elucidate the dispersion and absorption of light energy based on the band gap and density of states, which represents the interaction of incident photons. The real part $\varepsilon_1(\omega)$ and the imaginary part $\varepsilon_2(\omega)$ of the dielectric function can be calculated using the following equations [47, 48]:

$$\varepsilon_1(\omega) = 1 + \frac{2}{\pi} P \int_0^{\infty} \frac{\omega' \varepsilon_2(\omega')}{\omega'^2 - \omega^2} d\omega' \tag{1}$$

$$\varepsilon_2(\omega) = \frac{2e^2\pi}{\Omega\varepsilon_0} \sum_{k,v,c} \left| \left\langle \psi_k^c \left| \hat{u} \cdot r \right| \psi_k^v \right\rangle \right|^2 \delta(E_k^c - E_k^v - E) \tag{2}$$

Here ω is the light frequency, e is the electronic charge, ψ_k^v and ψ_k^c are the valence and conduction band wave functions at wave vector k, respectively.

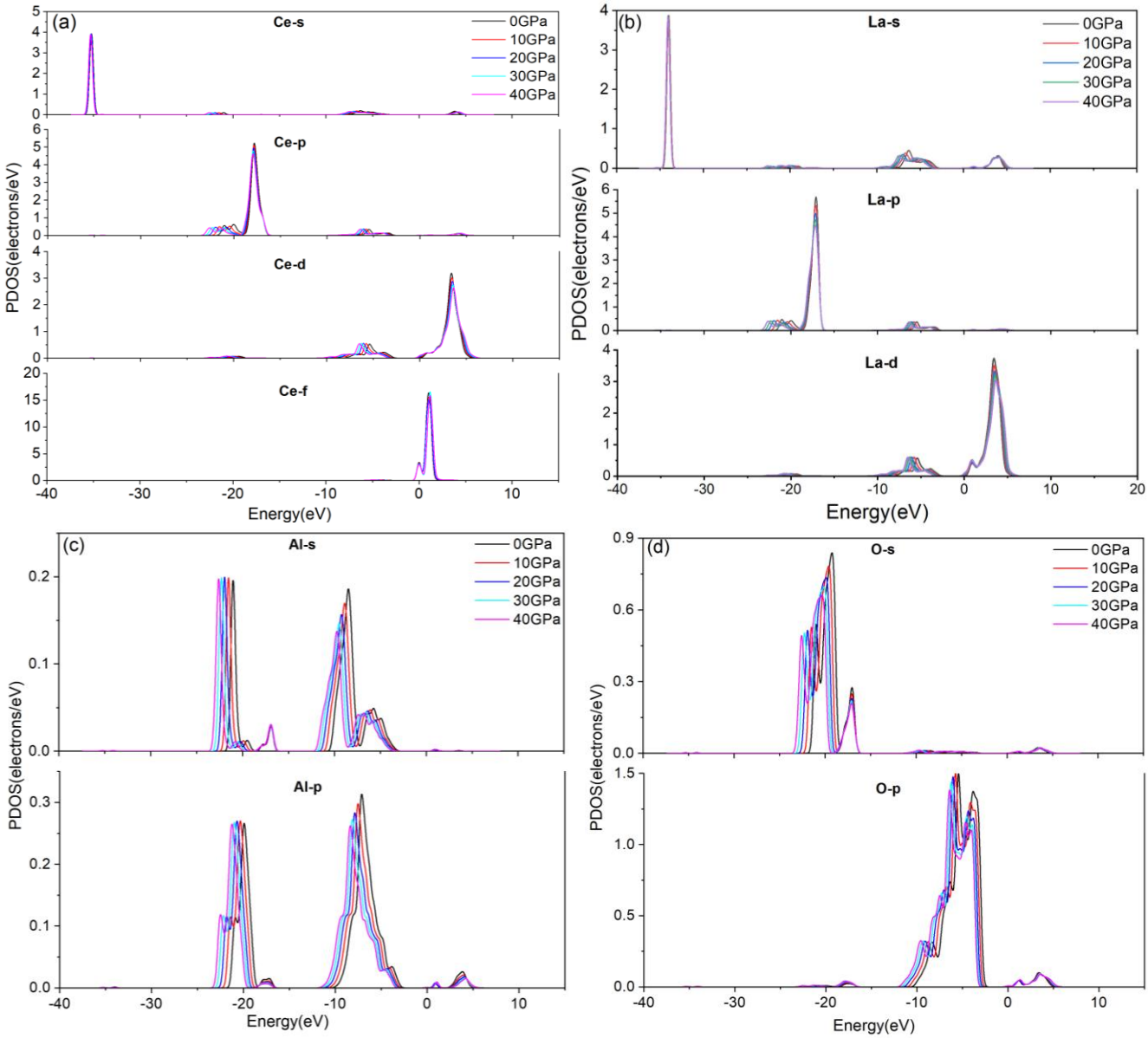

Fig. 5. Partial density of states for (a) Ce, (b) La, (c) Al and (d) O under different pressures (colour online)

Fig. 6 shows the effect of pressure on the complex dielectric function of cubic $Ce_{0.5}La_{0.5}AlO_3$. From Fig. 6a, the static dielectric constant presents the slow upward trend with the increase of the pressure, which is exactly opposite to the variation of the band gap with the increasing pressure and is in excellent agreement with Penn's model [30, 49]. Under the different pressures, the value of the real part of the dielectric function $\varepsilon_1(\omega)$ increases rapidly from zero frequency and then drops sharply. Fig. 6a also displays the metallic nature of $Ce_{0.5}La_{0.5}AlO_3$ when the value of the real part of the dielectric function $\varepsilon_1(\omega)$ becomes negative at around 7.6 eV. It is well-known that the value of the imaginary part of the dielectric function $\varepsilon_2(\omega)$ represented the attenuation of light discloses the absorption rate of electromagnetic waves. Fig. 6b shows that the imaginary part of the dielectric function $\varepsilon_2(\omega)$ of $Ce_{0.5}La_{0.5}AlO_3$ at ambient pressure starts to absorb light at 2.55 eV, which is consistent with the previously calculated band gap due to the compatibility between the energy of incident light and the band gap of the material. As photon energy increases, two major absorption peaks are observed at about 7.31 eV and 21.16 eV for cubic $Ce_{0.5}La_{0.5}AlO_3$ at ambient pressure, indicating strong light absorption. It is evident that the intensity of the strongest peak of $\varepsilon_2(\omega)$ increases with increasing pressure.

As widely recognized, the absorption coefficient $\alpha(\omega)$, the reflectivity $R(\omega)$, and the energy-loss function $L(\omega)$ can be achieved by the complex dielectric function, as followed [50]:

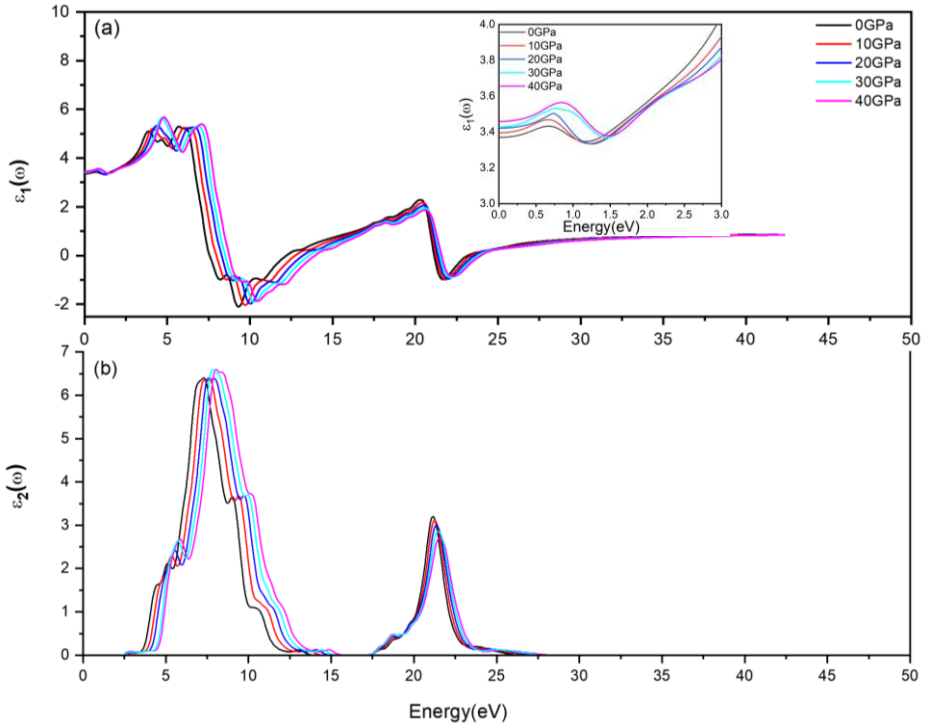

Fig. 6. Variations of the (a) real part and (b) imaginary part of the dielectric constant with different pressures for $Ce_{0.5}La_{0.5}AlO_3$. The inset shows the edge of real part of the dielectric constant (colour online)

$$\alpha(\omega) = \sqrt{2}\omega\left[\sqrt{\varepsilon_1(\omega)^2 + \varepsilon_2(\omega)^2} - \varepsilon_1(\omega)\right]^{1/2} \quad (3)$$

$$R(\omega) = \left|\frac{\sqrt{\varepsilon(\omega)} - 1}{\sqrt{\varepsilon(\omega)} + 1}\right|^2 \quad (4)$$

$$L(\omega) = \varepsilon_2(\omega)/\left[\varepsilon_1(\omega)^2 + \varepsilon_2(\omega)^2\right] \quad (5)$$

The absorption coefficient $\alpha(\omega)$ can describe the decay of light, and the critical values of $\alpha(\omega)$ and $\varepsilon_2(\omega)$ may present the optical band gap. Fig. 7 shows the $\alpha(\omega)$ of $Ce_{0.5}La_{0.5}AlO_3$ under different pressures according to the Eq. (3) [50]. The two prominent absorption peaks for cubic $Ce_{0.5}La_{0.5}AlO_3$ represent the changes in the rates of intraband transition and interband transition, and both the absorption peaks shift toward higher energy with increasing pressure [51].

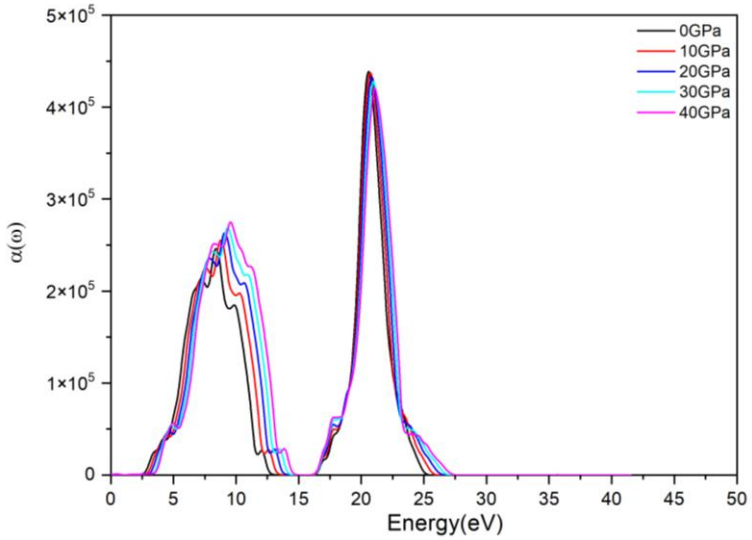

Fig. 7. Variation of the absorption coefficient with different pressures for $Ce_{0.5}La_{0.5}AlO_3$ (colour online)

According to the Eq. (4) [50], the influence of pressure on the $R(\omega)$ of cubic $Ce_{0.5}La_{0.5}AlO_3$ is presented in Fig. 8. All the values of $R(\omega)$ have undergone large fluctuation owing to the different rate of electron transitions. Due to the metallicity of $Ce_{0.5}La_{0.5}AlO_3$, the reflectivity rapidly increases from zero frequency to its maximum value, which corresponds to the real part of the dielectric constant being close to zero. With the increase of pressure, a significant blue-shift has also been observed in Fig. 8 for the peaks of $R(\omega)$ of $Ce_{0.5}La_{0.5}AlO_3$.

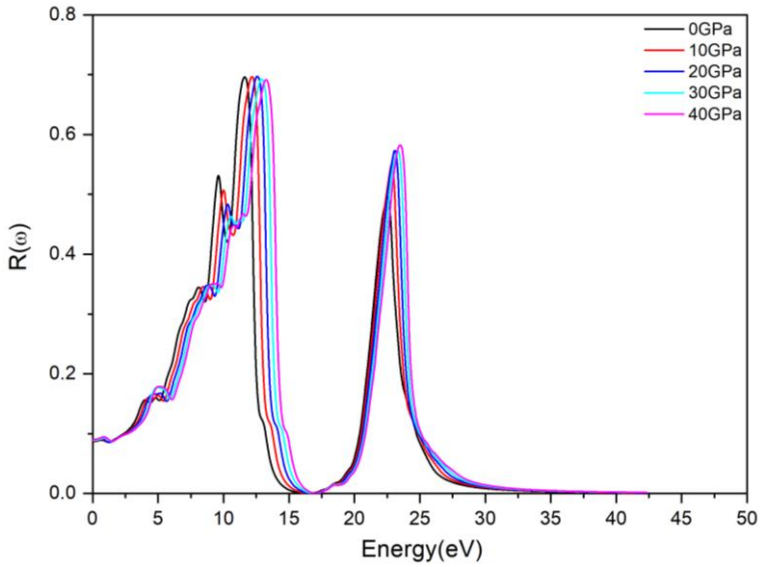

Fig. 8. Variation of the reflectivity with different pressures for $Ce_{0.5}La_{0.5}AlO_3$ (colour online)

In addition, the value of $L(\omega)$ closely related to heating, scattering, and other resistive effects reveals the energy loss of fast electrons when passing through materials [52]. As electrons are excited by light, they are not limited to their natural lattice sites and will generate plasma oscillations. The main peak of $L(\omega)$, known as the bulk plasma frequency indicates the sharp decline of $R(\omega)$ and happens at $\varepsilon_2(\omega)<1$ and $\varepsilon_1(\omega)$ tends to zero [53]. In Fig. 9, there are two plasmonic peaks for $Ce_{0.5}La_{0.5}AlO_3$ at ambient pressure and the sharpest one is located at 10.77 eV. Both peaks of energy-loss function obtained for $Ce_{0.5}La_{0.5}AlO_3$ exhibit a blue-shift with increasing pressure.

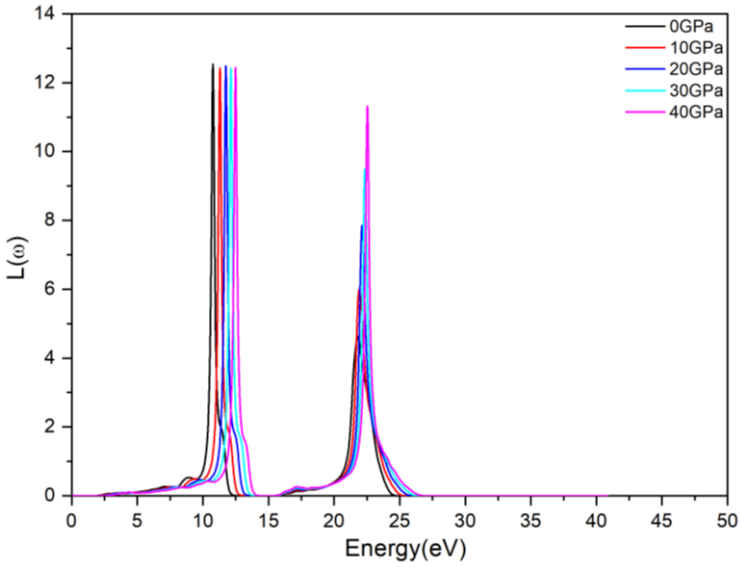

Fig. 9. Variation of the energy-loss function with different pressures for $Ce_{0.5}La_{0.5}AlO_3$ (colour online)

4. Conclusions

This DFT-based investigation with the Heyd-Scuseria-Ernzerhof screened hybrid functional clarified how the pressure modulated the core properties of cubic $Ce_{0.5}La_{0.5}AlO_3$, delivering findings critical for both fundamental research and practical applications. Structurally, increasing pressure led to a significant reduction in the lattice constant. It was driven by enhanced atomic motion that shortens interatomic distances, which in turn served as the basis for subsequent changes in electronic and optical behaviors. Electronically, the band gap decreased continuously with pressure. The detailed analyses with TDOS and PDOS further revealed that pressure increased the bandwidths of the middle valence band, high valence band, and conduction band, while the low valence band remained unchanged. Optically, pressure induced multiple key effects. It raised the static dielectric constant, strengthened the intensity of the strongest peak in the imaginary part of the dielectric function, and triggered clear blue-shifts in the major peaks of the absorption coefficient, reflectivity, and energy-loss function. These results confirmed pressure as an effective tuning parameter for the properties of $Ce_{0.5}La_{0.5}AlO_3$. Given the material's relevance to scintillators and optoelectronics, this work offered essential guidance for optimizing its performance in pressure-sensitive devices, while also laid the groundwork for future experimental validation and expanded application development.

Acknowledgments

This work was supported by the Science and Technology Research Project of Education Department of Hubei Province under Grant No. B2015014.

References

[1] M. J. Ferrari, M. Johnson, F. C. Wellstood, J. Clarke, A. Inam, X. D. Wu, L. Nazar, T. Venkatesan, Nature **341**(6244), 723 (1989).
[2] A. E. Lee, C. E. Platt, J. F. Burch, R. W. Simon, J. P. Goral, M. M. Al-Jassim, Appl. Phys. Lett. **57**(19), 2019 (1990).
[3] R. W. Simon, C. E. Platt, A. E. Lee, G. S. Lee, K. P. Daly, M. S. Wire, J. A. Luine, M. Urbanik, Appl. Phys. Lett. **53**(26), 2677 (1988).
[4] Y. Gim, T. Hudson, Y. Fan, C. Kwon, A. T. Findikoglu, B. J. Gibbons, B. H. Park, Q. X. Jia, Appl. Phys. Lett. **77**(8), 1200 (2000).
[5] R. Spinicci, P. Marini, S. D. Rossi, M. Faticanti, P. Porta, J. Mol. Catal. A-Chem. **176**(1-2), 253 (2001).
[6] Z. Q. Liu, S. Y. Chiam, W. K. Chim, J. S. Pan, C. M. Ng, J. Electrochem. Soc. **157**(12), G250 (2010).
[7] B. E. Park, H. Ishiwara, Appl. Phys. Lett. **82**(8), 1197 (2003).
[8] D. A. Atwood, B. C. Yearwood, J. Organometallic Chemistry **600**(1-2), 186 (2000).
[9] T. Takahashi, H. Iwahara, Energy Conversion **11**(3), 105 (1971).
[10] Y. Xu, A. Goyal, N. A. Rutter, D. Shi, M. Paranthaman, S. Sathyamurthy, P. M. Martin, D. M. Kroeger, J. Mater. Res. **18**(3), 677 (2003).
[11] M. Nikl, A. Yoshikawa, Adv. Opt. Mater. **3**(4), 463 (2015).
[12] M. J. Weber, J. Appl. Phys. **44**(7), 3205(1973).
[13] X. Zeng, L. Zhang, G. Zhao, J. Xu, H. Yin, H. Pang, Jie, C. Yan, X. He, J. Cryst. Growth **271**(1-2), 319 (2004).
[14] S. G. Lim, S. Kriventsov, T. N. Jackson, J. H. Haeni, D. G. Schlom, A. M. Balbashov, R. Uecker, P. Reiche, J. L. Freeouf, G. Lucovsky, J. Appl. Phys. **91**(7), 4500 (2002).
[15] X. B. Lu, Z. G. Liu, Y. P. Wang, Y. Yang, X. P. Wang, H.W. Zhou, B.Y. Nguyen, J. Appl. Phys. **94**(2), 1229 (2003).
[16] J. Y. Park, G. M. Choi, Solid State Ionics **154**, 535 (2002).
[17] P. J. Deren, R. Mahiou, Opt. Mater. **29**(7), 766 (2007).
[18] M. Losurdo, M. M. Giangregorio, M. Luchena, P. Capezzuto, G. Bruno, R. G. Toro, G. Malandrino, I. L. Fragalà, R. L. Nigro, Appl. Surf. Sci., **253**(1), 322 (2006).
[19] A. A. Demkov, X. D. Zhang, H. Loechelt, R. Liu, Journal of Vacuum Science and Technology B **18**(5), 2388 (2000).
[20] H. Wadati, Y. Hotta, A. Fujimori, T.M. Susaki, H. Y. Hwang, Y. Takata, K. Horiba, M. Matsunami, S. Shin, M. Yabashi, Phys. Rev. B **77**(4), 045122 (2008).
[21] R. Devine, J. Appl. Phys. **93**(12), 9938 (2003).
[22] V. V. Afanas'ev, A. Stesmans, C. Zhao, M. Caymax, T. Heeg, J. Schubert, Y. Jia, D. Schlom, G. Lucovsky, Appl. Phys. Lett. **85**(24), 5917 (2004).
[23] B. E. Park, H. Ishiwara, Appl. Phys. Lett. **79**(6), 806 (2001).
[24] Y. Y . Mi, Z. Yu, S. J. Wang, P. C. Lim, Y. L. Foo, A. C. H. Huan, C. K. Ong, Appl. Phys. Lett. **90**(18), 181925 (2007).
[25] V. Garcia, M. Bibes, J. L. Maurice, E. Jacquet, K. Bouzehouane, J. P. Contour, A. Barthelemy, Appl. Phys. Lett. **87**(21), 212501 (2005).
[26] E. Cicerrella, J. L. Freeouf, L.F. Edge, D. G. Schlom, T. Heeg, J. Schubert, S. A. Chambers, Journal of Vacuum Science and Technology A **23**(6), 1676 (2005).
[27] A. A. Knizhnik, I. M. Iskandarova, A. A. Bagatur-Yants, B. V. Potapkin, L. R. C. Fonseca, A. Korkin, Phys. Rev. B **72**(23), 235329 (2005).
[28] P. Delugas, V. Fiorentini, A. Filippetti, Phys. Rev. B **71**(13), 134302 (2005).
[29] P. W. Peacock, J. Robertson, J. Appl. Phys. **92**(8), 4712 (2002).
[30] K. Xiong, J. Robertson, S. Clark, Appl. Phys. Lett. **89**(2), 022907 (2006).
[31] J. Pejchal, J. Barta, T. Trojek, R. Kucerkova,

A. Beitlerova, M. Nikl, Meas. **121**, 26 (2019).
[32] V. Laguta, M. Buryi, J. Pejchal, K. Uličná, V. Římal, V. Chlan, H. Štěpánková, Yu. Zagorodniy, M. Nikl, Journal of Solid State Chemistry **333**, 123295 (2022).
[33] L. Vasylechkoa, A. Senyshyn, D. Trots, R. Niewa, W. Schnelle, M. Knapp, Journal of Solid State Chemistry **180**(4), 1277 (2007).
[34] A. Bouhemadou, R. Khenata, F. Djabi, Solid State Sciences **11**(2), 556 (2009).
[35] S. Liu, H. Zhang, L. Wang, J. Chen, Journal of Physics: Condensed Matter **34**(15), 155401(2022).
[36] J. P. Perdew, K. Burke, M. Ernzerhof, Phys. Rev. Lett. **77**(18), 3865 (1996).
[37] T. Van, Khanh, N. T. T. Linh, P. Ha, Trinh, H. K. Phung, N. T. Tung, T. T. Trung, Chiang Mai Journal of Science **49**(5), 1324 (2022).
[38] R. L. Martin, F. Illas, Phys. Rev. Lett. **79**(8), 1539 (1997).
[39] T. Bredow, A. Gerson, Phys. Rev. B **61**(8), 5194 (2000).
[40] J. Muscat, A. Wander, N. M Harrison, Chem. Phys. Lett. **342**(3-4), 397 (2001).
[41] J. K. Perry, J. Tahir-Kheli, W. A. Goddard, Phys. Rev. B **63**(14), 144510 (2001).
[42] K. N. Kudin, G. E. Scuseria, R. L. Martin, Phys. Rev. Lett. **89**(26), 266402 (2002).
[43] P. J. Hay, R. L. Martin, J. Uddin, G. E. Scuseria, J. Chem. Phys. **125**(3), 034712 (2006).
[44] J. Heyd, G. E. Scuseria, M. Ernzerhof, J. Chem. Phys. **118**(18), 8207 (2003).
[45] W. Zhao, X. Chen, S. Liu, H. Wang, J. Li, Q. Zhang, Y. Yang, Y. He, Computational Materials Science **225**, 112289 (2023).
[46] T. Liu, Y. He, Q. Zhang, H. Wang, J. Li, Y. Yang, Phys. Rev. B **104**(16), 165138 (2021).
[47] C. Li, B. Wang, R. Wang, H. Wang, X. Y. Lu, Physica B **403**(4), 539 (2008).
[48] S. M. Hosseini, Physica B **403**(10-11), 1907 (2008).
[49] J. Chen, X. Wang, Z. Li, H. Zhang, Y. Liu, Q. Yang, Journal of Physics: Condensed Matter **37**(12), 125402 (2025).
[50] S. Saha, T. P. Sinha, A. Mookerjee, Phys. Rev. B **62**, 8828 (2000).
[51] F. Peng, D. Yao, L. Sun, Y. Liu, H. Zhang, Q. Wang, Thin Solid Films **795**, 141980 (2024).
[52] A. Bouhemadou, R. Khenata, Comput. Mater. Sci. **39**(4), 803 (2007).
[53] R. Saniz, L. H. Ye, T. Shishidou, A.J. Freeman, Physical Review B **74**(1), 014209 (2006).

*Corresponding author: lidanhanadusi@163.com